Ca^{2+}/H^{+} exchange by acidic organelles regulates cell migration in vivo

Manuela Melchionda,[1] Jon K. Pittman,[2] Roberto Mayor,[1] and Sandip Patel[1]

[1]Department of Cell and Developmental Biology, University College London, London WC1E 6BT, England, UK
[2]Faculty of Life Sciences, University of Manchester, Manchester M13 9PT, England, UK

Increasing evidence implicates Ca^{2+} in the control of cell migration. However, the underlying mechanisms are incompletely understood. Acidic Ca^{2+} stores are fast emerging as signaling centers. But how Ca^{2+} is taken up by these organelles in metazoans and the physiological relevance for migration is unclear. Here, we identify a vertebrate Ca^{2+}/H^{+} exchanger (CAX) as part of a widespread family of homologues in animals. CAX is expressed in neural crest cells and required for their migration in vivo. It localizes to acidic organelles, tempers evoked Ca^{2+} signals, and regulates cell-matrix adhesion during migration. Our data provide new molecular insight into how Ca^{2+} is handled by acidic organelles and link this to migration, thereby underscoring the role of noncanonical Ca^{2+} stores in the control of Ca^{2+}-dependent function.

Introduction

Cell migration is vital for morphogenesis, wound healing, and immune response (Ridley et al., 2003). It involves a series of coordinated events that include attachment to the substratum, formation of protrusions in a polarized manner, and retraction of the trailing end of the cell. Focal adhesions are transient macromolecular complexes that link the cell cytoskeleton to the extracellular substratum and are thus essential for migration. Deregulated migration underlies many disorders including cancer, thus highlighting the need to precisely define how migration is regulated (Spano et al., 2012).

Ca^{2+} is a widespread signaling ion that mediates its effects through spatially and temporally complex Ca^{2+} signals (Berridge et al., 2003). These signals are generated by the interplay between Ca^{2+} channels, which mediate elevations in cytosolic Ca^{2+} and pumps/exchangers, which both temper these elevations and fill Ca^{2+} stores. During migration, Ca^{2+} gradients form in the cytosol, whereby Ca^{2+} levels are lower at the leading edge, likely due to enhanced plasma membrane Ca^{2+} ATPase activity (Brundage et al., 1991; Tsai et al., 2014). Much attention has focused on the role of Ca^{2+} influx in regulating cell migration. In particular, key roles for both store- and mechanically operated Ca^{2+} influx have emerged, and localized Ca^{2+} release events at the leading edge have been resolved (Evans and Falke, 2007; Wei et al., 2009; Yang et al., 2009; Tsai and Meyer, 2012). Relatively little is known about the role of intracellular Ca^{2+} stores in regulating cell migration.

It is now clear that a variety of acidic organelles, such as lysosomes and lysosome-related organelles, store Ca^{2+} that can be mobilized to regulate Ca^{2+}-dependent functions (Christensen et al., 2002; Churchill et al., 2002; Patel and Docampo, 2010). However, there is limited information concerning the molecular basis for Ca^{2+} handling by these so-called acidic Ca^{2+} stores (Patel and Muallem, 2011) despite links to disease (Lloyd-Evans et al., 2008). In particular, although recent work has defined the molecular basis for Ca^{2+} release from acidic organelles (e.g., the identification of organellar Ca^{2+} release channels; Patel, 2015), there is currently a paucity of information regarding the molecular basis for Ca^{2+} uptake. Better understood is uptake of Ca^{2+} by plant, fungal, and protist vacuoles, acidic organelles that are often likened to lysosomes in animal cells. Vacuolar Ca^{2+} uptake is mediated in part by Ca^{2+}/H^{+} exchangers (CAXs; Pittman, 2011). CAXs belong to the Ca^{2+}/cation antiporter superfamily of exchangers and use the substantial proton gradient across the vacuole membrane to drive low affinity, high capacity antiport of Ca^{2+} into the lumen (Hirschi et al., 1996). Deletion of CAX genes impairs Ca^{2+} homeostasis and physiological function such as gas exchange, growth, and fitness in plants (Cheng et al., 2005; Conn et al., 2011) and stress responses in yeast (Denis and Cyert, 2002). Although filling of acidic organelles by Ca^{2+}/H^{+} exchange is likely ubiquitous in animals (Patel and Docampo, 2010), molecular interrogation is almost completely unexplored (Manohar et al., 2010), possibly because of the assumption that CAX genes are not widespread in metazoans.

Here, we identify animal CAXs and reveal an essential role for them in the migration of the neural crest, a highly migratory embryonic cell population fated to differentiate into a wide range of cell types (Mayor and Theveneau, 2013).

Correspondence to Roberto Mayor: r.mayor@ucl.ac.uk; or Sandip Patel: patel.s@ucl.ac.uk

Abbreviations used in this paper: CAX, Ca^{2+}/H^{+} exchanger; GPN, glycylphenylalanine2-naphthylamide.

The Rockefeller University Press $30.00
J. Cell Biol. Vol. 212 No. 7 803–813
www.jcb.org/cgi/doi/10.1083/jcb.201510019

Results and discussion

CAXs are widespread in the animal kingdom

Database searches using plant and yeast CAX sequences as queries retrieved multiple putative CAX genes across the animal kingdom (Fig. 1 and Table S2). Animal CAXs were characterized by the core CAX domain with 11 predicted transmembrane regions and an N-terminal extension harboring a domain of unknown function with an additional two predicted transmembrane regions (Fig. 1 a). In protostomes, putative CAX genes were represented in molluscs such as the California sea hare (a gastropod) and Annelids such as the polychaete worm (Fig. 1 b). CAX genes were also found in deuterostomes, as evinced by their presence in echinoderms such as the sea urchin and a number of chordates. The latter spanned basal organisms exemplified by the lancelet and both ray-finned fish (e.g., the teleosts, which possessed two CAX genes; Manohar et al., 2010) and lobe-finned fish (e.g., the coelacanths). CAX genes were also present in amphibians, reptiles, and birds. Intriguingly, we additionally identified CAX sequences in two mammals, namely the platypus and the Tasmanian devil (Fig. 1 b), although CAXs appeared to be absent in placental mammals.

A clone harboring the complete open reading frame of sea urchin (*Stronglylocentrotus purpuratus*) CAX was isolated by RT-PCR from eggs (Fig. 1 c). We also identified an expressed sequence tag corresponding to the full-length sequence of CAX from the frog (*Xenopus laevis*), a tractable model system for the study of cell migration in vivo (Carmona-Fontaine et al., 2008). Embryonic expression was confirmed by RT-PCR (Fig. 1 c). Molecular cloning of CAX from representative invertebrate and vertebrate species thus validates the widespread occurrence of CAXs. Multiple sequence alignment and structural modeling of *Xenopus* CAX indicates conservation of acidic residues in the α1 and α2 repeats of CAXs implicated in coordinating Ca^{2+} ions during the transport cycle and overall core domain structure (Fig. 1, d and e; Waight et al., 2013).

To assess transporter function, we expressed *Xenopus* CAX in yeast. In a mutant strain lacking both yeast CAX (VCX1) and the vacuolar Ca^{2+} ATPase, PMC1 (*Δvcx1Δpmc1*), total Ca^{2+} content was reduced about twofold relative to wild-type yeast (Fig. 1 f). In this double mutant background, which was necessary because of functional redundancy (Cunningham and Fink, 1994), Ca^{2+} content was increased upon expressing wild-type CAX. In contrast, expressing CAX lacking the N terminus (CAXΔN) had little effect, suggesting a requirement for the N terminus in CAX action. We also mutated conserved E^{420} in the α1 repeat (Fig. 1 d). Like CAXΔN, CAX^{E420A} was also inactive (Fig. 1 f). To demonstrate transporter function more directly, we measured Ca^{2+}/H^+ exchange activity in subcellular fractions by monitoring Ca^{2+}-dependent changes in luminal pH. For these experiments, we used a yeast strain devoid of endogenous CAX activity (*Δvcx1Δvnx*). As shown in Fig. 1 g, wild-type CAX restored Ca^{2+}/H^+ activity, whereas CAXΔN and CAX^{E420A} did not.

In summary, we identify an expanded family of bona fide CAXs in animals indicating that these transporters are much more widespread in Metazoa than previously assumed.

CAX regulates cell migration in vivo

In situ hybridization analyses of *Xenopus* embryos revealed enriched staining for CAX in the neural crest (Fig. 2 a). Neural crest cells are a highly motile embryonic cell population that form at the border of the neural plate and subsequently migrate throughout the embryo. To examine the effects of CAX on migration, CAX expression was manipulated with two validated antisense morpholinos (Fig. S1, a and b). Both induced a strong dose-dependent inhibition of neural crest migration, as analyzed by the expression of the neural crest markers *Twist* or *Snail2* (Fig. 2, b and c). However, neural crest induction was not affected (Fig. S1 c), indicating a specific requirement of CAX in migration.

To determine the specificity of the knockdown, we performed rescue experiments with GFP-tagged CAX. As shown in Fig. 2 d, there was a mild but significant rescue of the defect quantified by measuring the length of the neural crest streams. Rescue was not complete, probably because overexpression of CAX alone also disrupted neural crest migration (Fig. 2 d). In summary, we reveal an unexpected requirement for CAX in migration of a highly migratory cell type in vivo.

CAX localizes to acidic organelles

To determine the subcellular localization of animal CAX, we performed ex vivo experiments with neural crest explants (Scarpa et al., 2015). Confocal microscopy of explants expressing GFP-CAX revealed a vesicular pattern of staining (Fig. 3 a). Remarkably, this staining largely overlapped with that of the yolk granules, which have long been suggested as acidic Ca^{2+} stores (Churchill et al., 2002). In addition, we noted smaller puncta-expressing CAX (Fig. 3 a). Imaging of live cells stained with a fluorescent acidotrope confirmed the acidic nature of both the large and small CAX-positive vesicles (Fig. 3 b).

In an independent approach, we expressed *Xenopus* CAX in human cells. As in neural crest cells, CAX localized to vesicular structures in SHSY5Y cells, HeLa cells, and primary cultured fibroblasts (Fig. 3, c–f). These structures were acidic (Fig. 3 d). Coexpression of CAX with LAMP1, a late endosome/lysosome marker, revealed colocalization indicating that CAX is likely expressed in the endolysosomal system (Fig. 3 e). In accordance, CAX colocalized with endogenous LAMP1 (Fig. 3 f). Taken together, these data indicate that CAX is localized to acidic organelles.

CAX regulates cytosolic Ca^{2+} signaling

CAXs are responsible for clearing of stimulus-evoked Ca^{2+} signals in plants and yeast (Pittman, 2011). To probe the functionality of animal CAXs, we took two approaches. In the first approach, we examined the effect of overexpressing CAX on changes in cytosolic Ca^{2+} concentration upon agonist stimulation. For these experiments, we used SHSY5Y cells loaded with the fluorescent Ca^{2+} indicator, Fura-2. As shown in Fig. 4 a, stimulation of cells with carbachol evoked robust Ca^{2+} signals. Similar results were obtained in transiently transfected cells expressing LAMP1 or neighboring untransfected cells in the same imaging field (Fig. 4 a). In contrast, both the area under the curve and the initial peak after stimulation were substantially reduced in cells expressing CAX, whereas basal Ca^{2+} levels were similar (Fig. 4, a and b).

To determine whether the effect of CAX on agonist-evoked signals was due to Ca^{2+} uptake into acidic organelles, we examined the effects of the lysosomotropic agent glycylphenylalanine2-naphthylamide (GPN), which permeabilizes organelles containing the acidic protease cathepsin C (Jadot et al., 1984). After pretreatment with GPN, carbachol-evoked Ca^{2+} signals were similar in LAMP1- and CAX-transfected cells (Fig. 4, c

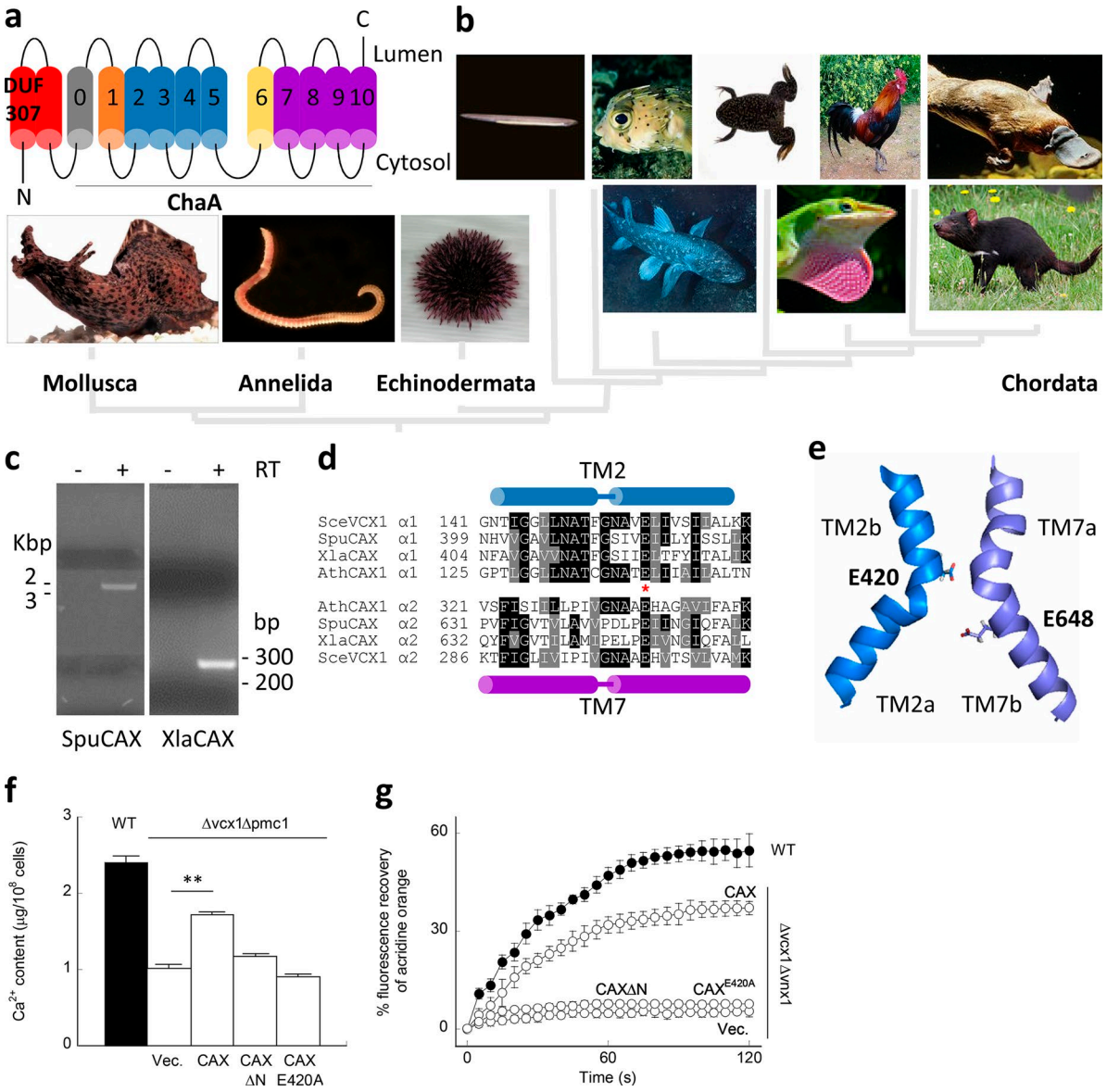

Figure 1. **CAXs are widespread in the animal kingdom.** (a) Proposed consensus topology of animal CAXs depicting a cytosolic N terminus, 13 transmembrane regions (cylinders), and a luminal C terminus. An N-terminal domain of unknown function (DUF 307) and a Ca^{2+}/H^+ antiporter (ChaA) domain comprising 11 transmembrane regions numbered 0–10 are highlighted. (b) CAX phylogeny in major metazoan phyla. Organisms depicted from left to right are *Aplysia californica*, *Capitella teleta*, *Strongylocentrotus purpuratus*, *Branchiostoma floridae*, *Takifugu rubripes*, *Latimeria chalumna*, *Xenopus tropicalis*, *Anolis carolinensis*, *Gallus gallus*, *Ornithorhynchus anatinus*, and *Sarcophilus harrisii*. See Table S2 for accession numbers. (c) Expression of animal CAXs. Agarose gel analysis of PCR reactions using primers specific for *S. purpuratus* (left) or *Xenopus* (right) CAX and templates prepared from RNA isolated from eggs and stage 16–18 embryos, respectively. Reactions were performed either with (+) or without (–) reverse transcription (RT). (d) Sequence comparison of animal, plant, and yeast CAXs. ClustalW2 multiple sequence alignment of TM2 and TM7 of the α1 and α2 repeats of CAX, respectively, from the sea urchin (SpuCAX), frog (XlaCAX), yeast (SceVCX1), and plant (AthCAX). *, glutamate residues conserved in both repeats. (e) Structural model of animal CAX. Magnified view of TM2 and 7 of *Xenopus* CAX highlighting E420 and E648, likely important for ion coordination. (f and g) Effect of CAX on Ca^{2+} homeostasis in yeast. (f) Inductively coupled plasma emission spectroscopy of total Ca^{2+} content. Data ($n = 9$) are from wild-type (WT) or *Δvcx1Δpmc1* yeast grown in 10 mM Ca^{2+} and transformed with empty vector (Vec.) or vectors expressing CAX, CAXΔN, and CAX^{E420A}. (g) Ca^{2+}/H^+ exchange measurements using endomembrane-enriched membrane vesicles and acridine orange fluorescence recovery in response to 50 μM Ca^{2+}. Data ($n = 4$ preparations) are from wild-type or *Δvcx1Δvnx1* yeast transformed with the indicated vector. Error bars represent SEM. **, $P < 0.01$.

and d). These data indicate a functional requirement for acidic organelles in CAX action and are consistent with localization of CAX to lysosomes in human cells (Fig. 2). Agonist-evoked Ca^{2+} signals were reduced in both populations relative to cells treated with vehicle, probably reflecting a requirement for Ca^{2+} release from acidic stores by carbachol. However, GPN-evoked cytosolic Ca^{2+} signals both before and after carbachol treatment were difficult to resolve (unpublished data).

CAX functionality was further explored by examining the effect of CAXΔN. For these experiments, we used C-terminally tagged CAX constructs. In contrast to wild-type CAX, CAXΔN was less effective in reducing agonist-evoked Ca^{2+} signals (Fig. 4, e and f). CAX^{E420A} was inactive (Fig. 4, e and f). These data mirror the activity of the CAX constructs in yeast (Fig. 1).

In the second approach, we probed the role of endogenous CAX in Ca^{2+} signaling in the neural crest. We measured cytosolic

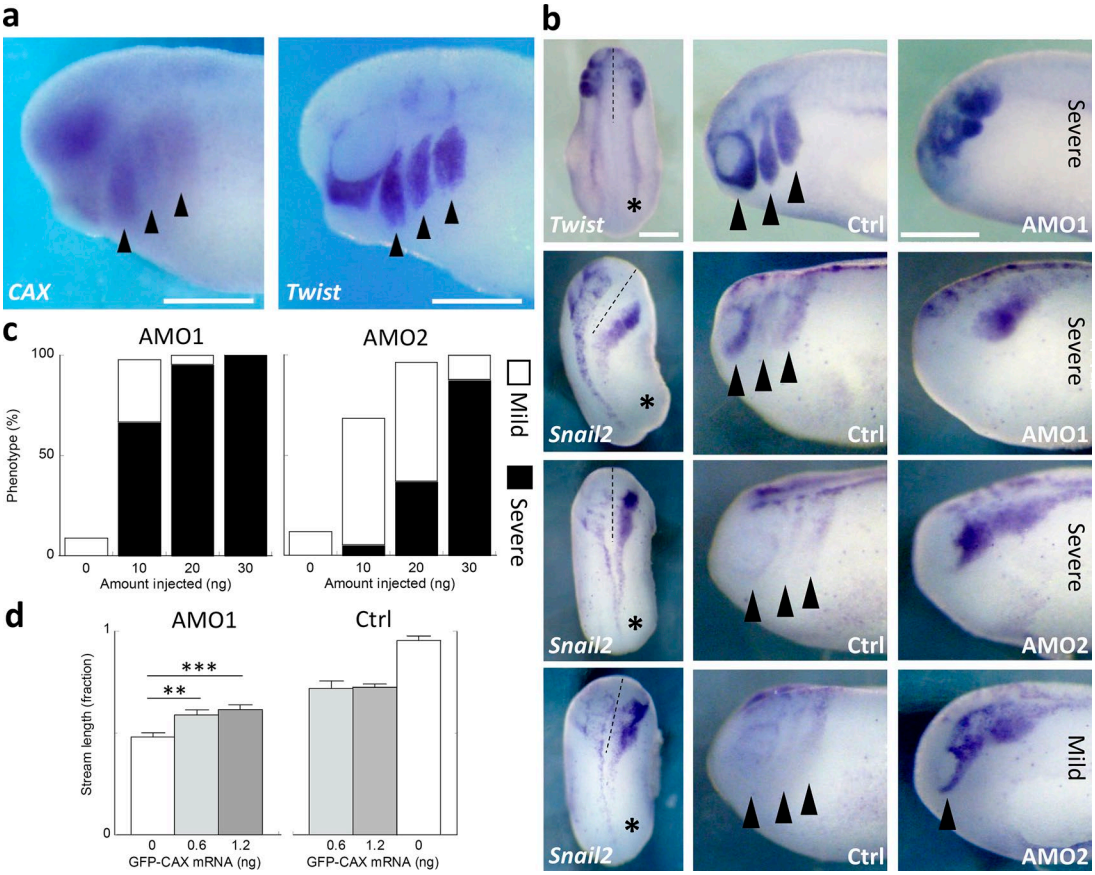

Figure 2. **CAX is required for cell migration in vivo.** (a) Tissue distribution of frog CAX. In situ hybridization of *CAX* and the neural crest marker *Twist* in stage 26/27 *Xenopus* embryos. Arrowheads mark the neural crest streams. (b–d) Effect of CAX knockdown on neural crest migration in vivo. (b) In situ hybridization analyses of *Twist* and the additional neural crest marker *Snail2* in exemplar stage 23/24 embryos injected with two antisense morpholinos (10 ng AMO1 or 20 ng AMO2). Dorsal views (left) and views along the anterior–posterior axis (right) for both the uninjected (control) and antisense morpholino–injected (*) sides of embryos (delineated by the dashed lines) are shown. Phenotypes were considered mild or severe. (c) Summary data quantifying the proportion of embryos displaying the indicated phenotype in response to increasing amounts of antisense morpholino. Results are from a single experiment where all six experimental manipulations were performed in parallel on the same batch of embryos (~1,000 injections). (d) Summary data from seven knockdowns (using 10 ng AMO1 and *Twist*) quantifying the length of all three neural crest streams, normalized to that in the uninjected side of the same embryo. Results are from CAX-depleted morphant embryos coinjected with increasing amounts of mRNA (0.6 or 1.2 ng; color coded) for GFP-CAX (left) or from control embryos injected with mRNA alone (right). Bars, 500 µm. Error bars represent SEM. **, $P < 0.01$; ***, $P < 0.001$.

Ca^{2+} levels using explants derived from embryos expressing the genetically encoded Ca^{2+} indicator, R-GECO. As shown in Fig. 4 (g and h), control embryos responded to carbachol, albeit weakly. However, in embryos depleted of CAX, responsiveness to carbachol was substantially enhanced. All cells from both sets of cultures responded to the Ca^{2+} ionophore, ionomycin, and the magnitude of the response in the CAX-depleted embryos was not different to those in control cultures (100 ± 15%; $n = 5$). These data are consistent with a role for CAXs in curbing Ca^{2+} signals in response to physiological stimulation (López-Sanjurjo et al., 2013), providing a corollary for our overexpression studies (Fig. 4, a–f). Collectively, the data presented in Fig. 4 further establish the functionality of CAX as a Ca^{2+} transporter and link activity to changes in cytosolic Ca^{2+}.

CAX regulates cell-substrate adhesion

Neural crest explants undergo directional migration to the chemokine Sdf-1 (Theveneau et al., 2010). Consistent with these data, control explants mounted a robust migratory response toward Sdf-1–soaked beads (Fig. 5 a and Video 1). CAX-depleted morphant explants also migrated toward Sdf-1. However, there was a delay before chemotaxis occurred (Video 1). Thus, the chemotactic index was more markedly reduced during the initial phase of recording in morphant explants relative to controls (Fig. 5, a and b). Persistence was also reduced; however, the velocity of migration was largely unaffected (Fig. 5 b). This suggested that CAX may affect an early step in the migratory response.

We also noted that morphant explants were consistently smaller than control embryos upon short-term culture (Fig. 5 c). This suggested that CAX might be involved in initial cell-spreading events. Indeed, morphant cells exhibited reduced dispersion (Fig. 5, d and e) and spreading (Fig. 5, f and g). Importantly, these effects were phenocopied by buffering intracellular Ca^{2+} with BAPTA (Fig. 5, h and i). Similar treatment with EGTA, however, was largely without effect. BAPTA and EGTA have similar affinities for Ca^{2+}, but BAPTA has a faster on-rate for Ca^{2+} binding. The differential effects of the two chelators on cell behavior therefore probably reflect the importance of local changes in Ca^{2+} (Stern, 1992).

The effect of CAX knockdown on cell dispersion and spreading suggests that neural crest cells fail to attach appropriately to the substrate. It is well known that attachment is dependent on focal adhesions, which are usually localized at the front

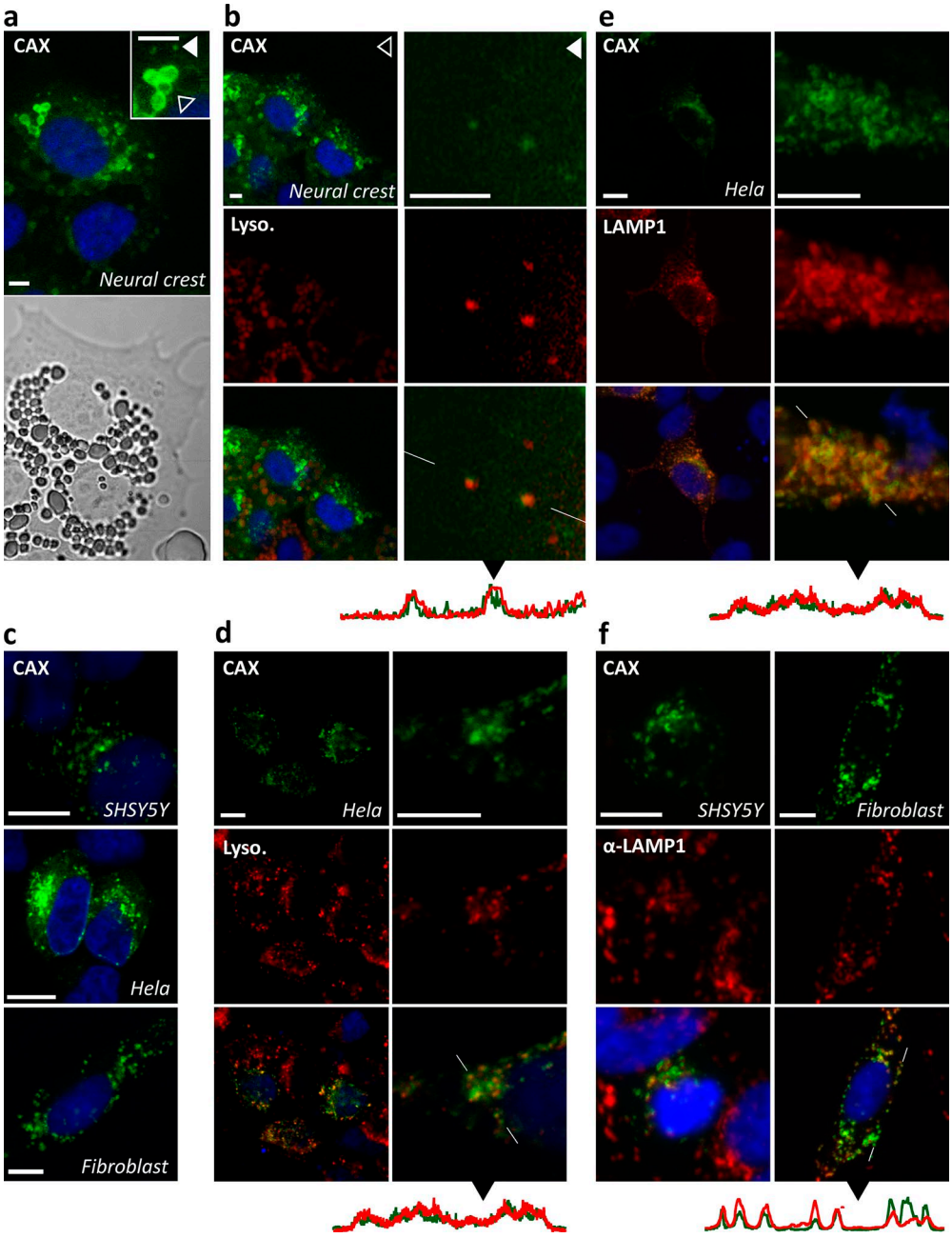

Figure 3. **CAX localizes to acidic organelles.** (a and b) Subcellular distribution of CAX in neural crest cells. (a) Confocal (top) and transmitted light (bottom) micrographs of exemplar neural crest cells expressing GFP-CAX. Inset shows a magnified image highlighting large (open triangles) and small (closed triangles) GFP-positive structures. (b) Images of GFP-CAX–expressing cells labeled with Lysotracker red (Lyso.). (Left) Images of large vesicles from cells loaded with 30 nM Lysotracker. (Right) Magnified images of small vesicles from independent cells loaded with 300 nM Lysotracker. Intensity plots of red and green fluorescence between the white lines in the overlaid image are shown below the images. (c–f) Subcellular distribution of CAX in human cells. (c) Confocal micrographs of the indicated cell type transiently transfected with GFP-CAX and fixed before imaging. (d) Distribution of GFP-CAX in live HeLa cells labeled with 100 nM Lysotracker red. (e) Distribution of GFP-CAX in fixed HeLa cells coexpressing LAMP1-mRFP. (f) Immunocytochemistry analysis using an antibody raised to LAMP1 in SHSY5Y cells or fibroblasts expressing GFP-CAX. Bars: (a and b) 5 µm; (c–f) 10 µm.

of the protrusions. Therefore, we analyzed the subcellular distribution of CAX during motility and compared it with the dynamics of focal adhesions. Time-lapse confocal imaging revealed that CAX-expressing vesicles were remarkably mobile and often moved into the cell protrusions (Fig. 5 j and Video 2). Imaging of cells coexpressing CAX and focal adhesion kinase placed the two in close proximity (Fig. 5 k and Video 3). This was quantified by the heat map in Fig. 5 k, which shows the distribution of CAX relative to the centroid of the focal adhesions. Continuous imaging of individual focal adhesions revealed prolonged association (>75 s) with CAX in 39% of the focal adhesions analyzed (Fig. S1 d), arguing against coincident colocalization.

Finally, we assessed whether focal adhesions were altered in morphant embryos. As shown in Fig. 5 (l and m), targeting of recombinant focal adhesion kinase was significantly reduced with respect to the number and size of labeled structures in the morphant explants. Staining of endogenous phosphopaxillin was similarly reduced (Fig. 5, l and m). Time-lapse imaging

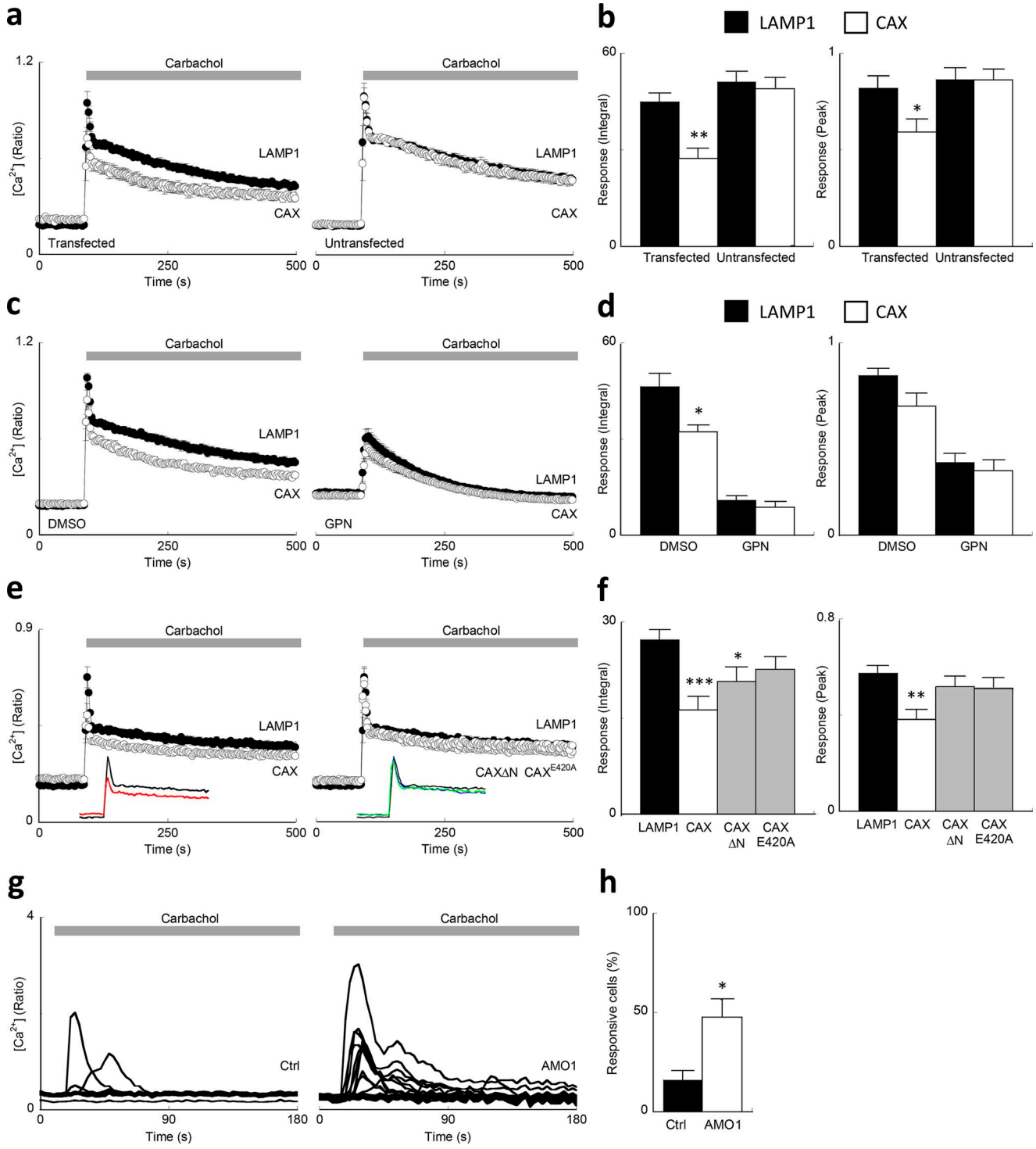

Figure 4. **CAX regulates cytosolic Ca^{2+} signaling.** (a–f) Effect of CAX overexpression on agonist-evoked Ca^{2+} signals. (a) Cytosolic Ca^{2+} levels of SHSY5Y cells loaded with the Ca^{2+} indicator Fura-2 and stimulated with 100 µM carbachol. Cells were from cultures transiently transfected with mRFP-CAX or LAMP1-mRFP, and data were segregated according to whether they were mRFP positive (transfected) or not (untransfected). (b) Pooled data (from seven transfections) quantifying the area under the curve (integral) and the peak response. (c) Effect of mRFP-CAX on carbachol-evoked Ca^{2+} signals in the presence of GPN. Cultures were treated with DMSO or 200 µM GPN for 30 min before stimulation. (d) Pooled data from four transfections. (e) Cytosolic Ca^{2+} responses of cells stimulated with 10 µM carbachol from cultures transiently transfected with LAMP1-mRFP, CAX-mRFP, CAXΔN-mRFP, or mRFP-CAX^{E420A}. Insets are expanded views of the initial responses presented as line plots without error bars (traces from cells expressing LAMP1 and the CAX mutants overlap). (f) Pooled data from six transfections. (g and h) Effect of CAX knockdown on agonist-evoked Ca^{2+} signals. (g) Cytosolic Ca^{2+} levels of neural crest cells expressing the Ca^{2+} indicator R-GECO1 and stimulated with 1 mM carbachol. Explants were from control embryos and embryos injected with 10 ng AMO1. (h) Pooled data from five knockdowns quantifying the proportion of cells that responded to agonist. Error bars represent SEM. *, $P < 0.05$; **, $P < 0.01$; ***, $P < 0.001$.

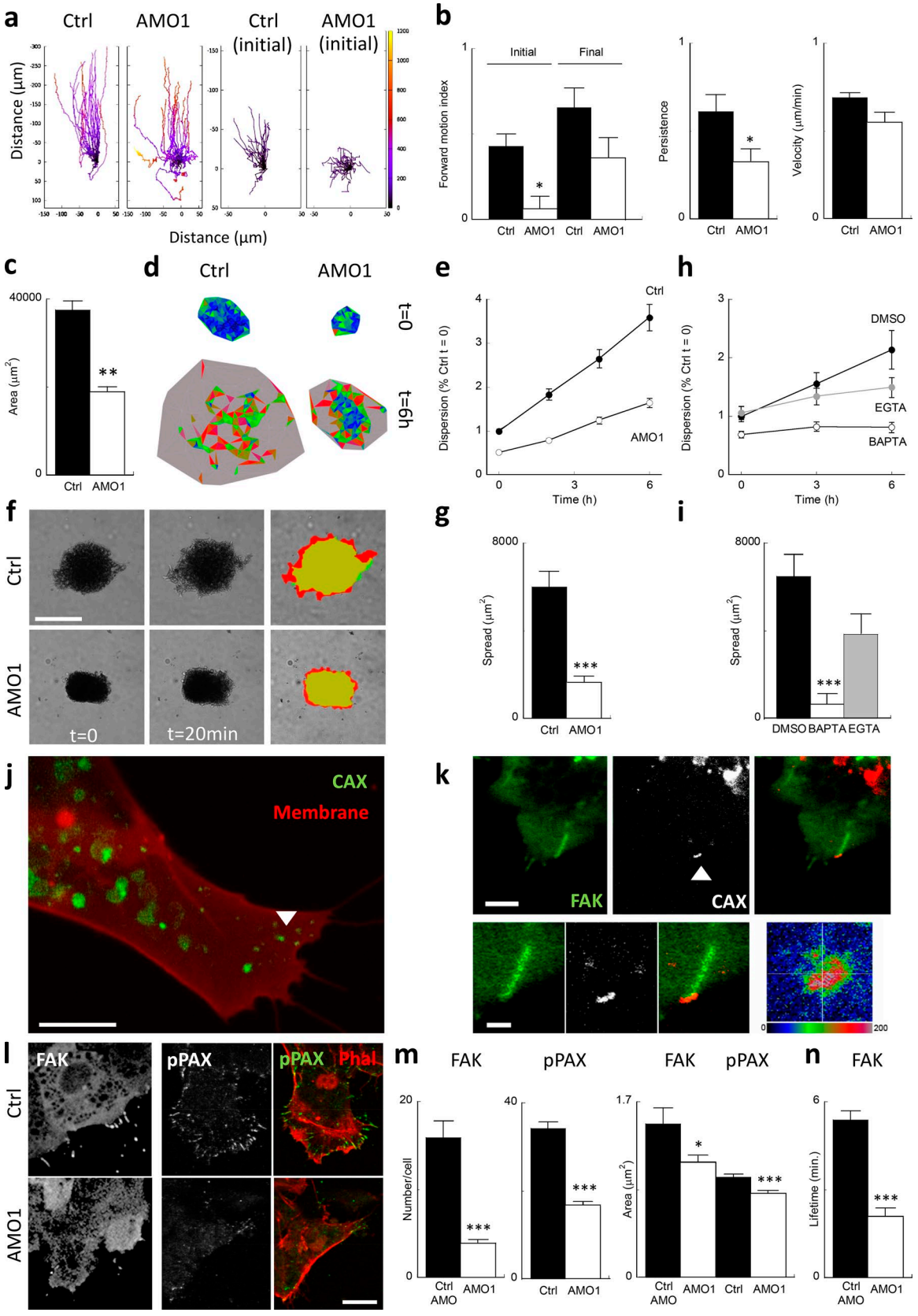

Figure 5. **CAX regulates cell substrate attachment.** (a and b) Effect of CAX knockdown on chemotaxis. (a) Tracks of individual explants migrating toward beads soaked in Sdf-1 over the entire period of recording (left) or the initial 100 min (right). (b) Summary data (from three knockdowns) quantifying forward motion index, persistence, and velocity of migration. (c–g) Effect of CAX knockdown on cell dispersion. (c) Summary data from three knockdowns quantifying the size of control and morphant explants 30 min after plating. (d) Representative color-coded triangulation diagrams at time 0 and 6 h from control or morphant explants. (e) Time courses (from three knockdowns) quantifying triangle area. Data are normalized to control explants at time 0.

of focal adhesions (Video 4) revealed that the lifetime of focal adhesions was decreased upon CAX knockdown (Fig. 5 n). Collectively, these data suggest that CAX is required for cell spreading and focal adhesion formation in a Ca^{2+}-dependent manner.

In summary, although release of Ca^{2+} from acidic organelles is increasingly appreciated as a critical cog in the Ca^{2+} signaling machine, the mechanism for Ca^{2+} uptake by these organelles, and the physiological relevance thereof, is unclear in metazoans. CAXs identified here join SERCA3 and TMEM165 as credible candidates for filling acidic organelles with Ca^{2+} (López et al., 2005; Demaegd et al., 2013). Importantly, Ca^{2+}/H^+ transport emerges as a novel way to control cellular migration and likely other Ca^{2+}-dependent events in animals.

Materials and methods

Bioinformatics

The protein databases at the National Center for Biotechnology Information were queried using BLAST and HMMER (Finn et al., 2015) with sequences of *Arabidopsis thaliana* CAX1 (GenBank accession no. AAL66749.1) and *Saccharomyces cerevisiae* CAX (Vcx1; RefSeq accession no. NP_010155.1). Multiple sequence alignments were performed using ClustalW2 or T-Coffee. Topology was predicted using TMpred, TMHMM 2.0, and TOPpred 1.10. For structural modeling, the C terminus of *Xenopus* CAX harboring the CAX domain (residues 305–570) was submitted to I-TASSER (Yang et al., 2015). The top ranked model based on the crystal structure of VCX1 (Protein Data Bank accession no. 4K1C) was selected. Structures were presented using Pymol.

Plasmids

Sea urchin CAX was cloned by PCR from *S. purpuratus* eggs using oligo-dT–primed cDNA prepared as described in Brailoiu et al. (2009). A 2.3-kb product was amplified using primers 5′-GCGAGGGGGACT TTTCACGTC-3′ (forward) and 5′-CGGCACGAGTGGGGCTTT AA-3′ (reverse), subcloned into TOPO TA, and sequenced in both directions. The predicted open reading frame (2,271 bp) was 98.6% identical to the coding sequence of a predicted transcript (RefSeq accession no. XM_782738). Frog CAX was amplified from *Xenopus* IMAGE clone 6640627 (RefSeq accession no. NM_001095931.1) harboring an open reading frame (2,253 bp) for hypothetical protein MGC115264.

For N-terminal tagging, the *Xenopus* CAX sequence was cloned into $pCS2^+$ into which the coding sequence of GFP and a flexible linker (GGSGGGGSGGGGSSG) separated by an SpeI site were inserted at the BamHI and EcoRI sites ($pCS2^+$ N GFP FL). For C-terminal tagging, CAX sequences were cloned into $pCS2^+$ into which the coding sequence of mRFP was inserted at the XhoI and XbaI sites ($pCS2^+$ C mRFP) as described in Brailoiu et al. (2009). Both plasmids were provided by M. Tada (University College London, London, England, UK).

A plasmid encoding N-terminally GFP-tagged CAX (GFP-CAX) was constructed by amplifying the open reading frame using primers (restriction sites underlined) 5′-ATTCGAATTCATGTCGCTGGAT GTGGAATAT-3′ (forward) and 5′-TCTCCTGTTGGCTGCTGATAT TCTAGAACTA-3′ (reverse) and cloning the product into the EcoRI and XbaI sites of $pCS2^+$ N GFP FL. A point mutant E420A was generated by site-directed mutagenesis of $pCS2^+$ N GFP FL CAX using the following mutagenic primers (mismatched nucleotides in italics): 5′-GCAACA TTTGGCTCCATTATTG*C*ACTGACCTTCTACATC-3′ (forward) and 5′-GATGTAGAAGGTCAGT*G*CAATAATGGAGCCAAATGTTGC-3′ (reverse). Plasmids encoding CAX tagged with mRFP at their N termini (both wild type and E420A) were generated by replacing the GFP sequence with mRFP in the corresponding N-terminally tagged GFP clones. This was achieved by amplifying the mRFP and upstream $pCS2^+$ vector sequence from $pCS2^+$ N mRFP described in Hooper et al. (2011) using primers 5′-CGGAGCAAGCTTGATTTAGG-3′ (forward) and 5′-TCCACCACTAGTGGCGCCGGTGGAGTG-3′ (reverse) and cloning the product at the HindIII–SpeI sites in $pCS2^+$ N GFP FL.

Wild-type (full length) and N-terminally truncated *Xenopus* CAX (lacking amino acids 1–316) were tagged at their C termini with mRFP (CAX-mRFP and CAXΔN-mRFP) by amplification using a common reverse primer (5′-CCATCTCCTGTTGGCTGCTCGAA TTCACTA-3′) and forward primers 5′-ATTCAGATCTATGTCGCTG GATGTGGAATAT-3′ and 5′-ATTCGGATCCATGGATGCATCATTT GATACCG-3′, respectively (restriction sites underlined). The products were cloned into the BamHI and EcoRI sites of $pCS2^+$ C mRFP.

For yeast expression, the open reading frames of CAX, CAX^{E420A}, and CAXΔN were amplified from their corresponding $pCS2^+$ plasmids and cloned into the XbaI and NotI sites of histidine selection yeast expression–integrating plasmid piHGpd (Nathan et al., 1999). This generated plasmids encoding untagged proteins under control of the constitutive GAPDH promoter. The following primer pairs were used (restriction sites underlined): 5′-AAATCTAGAATGTCGCTGGATGTGGAA TATG-3′ (forward) and 5′-AAAGCGGCCGCTCAGCAGCCAACAGG AGATG-3′ (reverse) for CAX and CAX^{E420A}, and 5′-AAATCTAGAATG GATGCATCATTTGATACCG-3′ (forward) and 5′-AAAGCGGCC GCTCAGCAGCCAACAGGAGATG-3′ (reverse) for CAXΔN.

The plasmid encoding membrane-targeted GFP was described in Carmona-Fontaine et al. (2008). Plasmids encoding R-GECO and GFP-tagged focal adhesion kinase were provided by N. Ueno (National Institute for Basic Biology, Okazaki, Japan) and T. Gomez (University of Wisconsin, Madison, WI; Robles and Gomez, 2006), respectively.

Yeast expression

S. cerevisiae strains K665 (*Δvcx1Δpmc1*) and OC06 (*Δvcx1Δvnx*; provided by O. Cagnac and K. Venema, Estación Experimental del Zaidín, Granada, Spain; Table S1) were transformed with empty piHGpd plasmid or piHGpd plasmids harboring CAX, CAXΔN, and CAX^{E420A} using the lithium acetate/polyethylene glycol method (Gietz and Schiestl, 2007) to generate K665 and OC06 strains each with

(f) Transmitted light micrographs showing spreading of control or morphant explants over a 20-min period. Panels on the right show an overlay of the area occupied by the explants where red represents the extent of spreading. Bar, 500 µm. (g) Summary data from three knockdowns quantifying spread area. (h and i) Effect of Ca^{2+} buffering on cell dispersion. Triangulation (h) and spreading (i) analysis of explants treated with cell-permeable Ca^{2+} chelators (50 µM BAPTA/EGTA-AM) or DMSO 30 min before imaging. (j and k) Live cell imaging of CAX. Stills from time-lapse confocal imaging of explants coexpressing mRFP-CAX and either membrane GFP (j; bar, 10 µm) or focal adhesion kinase–GFP (k). Arrowheads mark small CAX-positive vesicles. (k) Bars: (top) 4 µm; (bottom) 1 µm. Heat map summarizes the mean projection for CAX-positive vesicles relative to the centroid of focal adhesions (intersection of white lines) within 5 × 5–µm regions of interest. Data are from 28 focal adhesions from two expression experiments. (l–n) Effect of CAX knockdown on focal adhesions. (l) Expression of focal adhesion kinase–GFP (left) and immunocytochemistry analysis using an antibody to phosphopaxillin (middle) in control and morphant explants. Overlays (right) show costaining of phalloidin. Bar, 20 µm. (m) Summary data (94–422 cells from two to three knockdowns) quantifying the number and size of labeled structures. (n) Lifetime analysis of focal adhesion kinase–GFP in control and morphant explants (30–58 focal adhesions from two knockdowns). 10 ng AMO1 was used for all knockdowns. Error bars represent SEM. *, $P < 0.05$; **, $P < 0.01$; ***, $P < 0.001$.

ectopically integrated $GAPDH_{promoter}$-CAX, $GAPDH_{promoter}$-CAXΔN, and $GAPDH_{promoter}$-CAX^{E420A}. A 1-ml aliquot of yeast cells grown for 16 h in yeast extract–peptone–dextrose medium was pelleted, washed in a buffer containing 0.1 M lithium acetate, 10 mM Tris-HCl, pH 8.0, and 1 mM EDTA, and incubated with 4 µg plasmid DNA, 0.1 mg denatured salmon sperm carrier DNA (Sigma-Aldrich), 33% (wt/vol) polyethylene glycol (PEG 3350; Sigma-Aldrich), and 0.1 M lithium acetate. After mixing, the cells were heat shocked by incubation at 42°C for 1 h while shaking and then transferred to 20°C, washed, and then resuspended in sterile water before selection growth. Selection was performed with synthetic defined medium minus histidine (SD-H; Takara Bio Inc.) by growth at 30°C on solid SD-H medium.

Xenopus expression

Xenopus embryos were injected at the two- to four-cell stage with various probes together with fluorescein- or rhodamine-dextran and cultured according to standard procedures. For subcellular localization experiments, embryos were injected with 300 pg GFP/mRFP-tagged CAX. For knockdown experiments, embryos were injected with 10–30 ng antisense morpholinos with or without mRNA for GFP-CAX (600 or 1,200 pg). A control morpholino (5′-CCTCTTACCTCAGTTACA ATTTATA-3′) and antisense morpholinos targeting the exon1–intron boundary (5′-GATAGGAAAAGAGTGTCTCACCGAA-3′; AMO1) or the translation start site (5′-GACATATTCCACATCCAGCGA CATC-3′; AMO2) of CAX were designed by and purchased from Genetools. The target sequences for AMO1 and AMO2 were TTCGgtgag acactcttttcctatc (intronic sequence in lowercase) and 5′-GATGTCGCTG GATGTGGAATATGTC-3′; (start site underlined), respectively. For Ca^{2+} imaging, embryos were coinjected with mRNA encoding R-GECO and GFP (600 pg each). For CAX imaging, embryos were coinjected with mRNAs for mRFP-CAX and either 500 pg membrane-targeted GFP or 200 pg GFP-tagged focal adhesion kinase. Explants of *Xenopus* neural crest were dissected from stage 18 embryos after removal of the superficial ectoderm and plated on fibronectin-coated Petri dishes in modified Danilchick's medium for 30 min before time-lapse recording or fixation.

Human cell culture and heterologous expression

SHSY5Y cells were maintained in a 1:1 mixture of DMEM/Ham's F12 media and 1% (vol/vol) nonessential amino acids (all from Invitrogen). HeLa and primary cultured human fibroblasts were maintained in DMEM. Media were supplemented with 10% (vol/vol) FBS, 100 U/ml penicillin, and 100 µg/ml streptomycin. Cells were cultured at 37°C in a humidified atmosphere with 5% CO_2. Cells were transfected with CAX constructs or LAMP1-mRFP using Fugene6 (SHSY5Y, HeLa) or Lipofectamine LTX (fibroblasts) according to the manufacturer's instructions.

Ca^{2+} content determination

Yeast strains were grown in SD-H medium containing 10 mM $CaCl_2$ and harvested after 3 d of growth. 10 ml of cells were sequentially washed by centrifugation (3,000 *g* for 5–10 min) in 1 mM EDTA and H_2O to remove external bound Ca^{2+}. Cell pellets were oven dried at 60°C for 24 h and digested in 0.5 ml of ultrapure concentrated nitric acid (67%) at 100°C for 3 h. Samples were diluted in water and analyzed by inductively coupled plasma emission spectroscopy (Optima 5300; PerkinElmer) using matrix-matched Specpure multielement plasma standard solution 4 (Alfa Aesae) for calibration.

Preparation of vacuolar-enriched endomembrane vesicles

Vacuolar-enriched endomembrane vesicles from the indicated yeast strains were isolated by purification of the microsomal fraction through a two-step sucrose gradient (Pittman and Hirschi, 2001). Yeast cells were grown in SD-H medium overnight at 30°C and then grown in a 2-liter volume of yeast extract–peptone–dextrose medium overnight at 30°C. Cell pellets were washed after centrifugation at 4,000 *g* for 10 min in a wash buffer (0.1 M Tris-HCl, pH 9.4, 50 mM 2-mercaptoethanol, and 0.1 M glucose) and then incubated at 30°C for 1 h in spheroplast preparation buffer (0.05% [wt/vol] Zymolyase 20T [AMS Biotechnology], 0.9 M sorbitol, 0.1 M glucose, 50 mM Tris-MES, pH 7.6, 5 mM DTT, and 0.5× synthetic dextrose media) with gentle shaking. Spheroplasts were centrifuged at 3,000 *g* for 10 min and washed in 1 M sorbitol, and the pellet was resuspended in homogenization buffer (50 mM Tris-MES, pH 7.6, 1.1 M glycerol, 1.5% [wt/vol] polyvinylpyrrolidone 40,000, 5 mM EGTA, 1× protease inhibitor cocktail [Sigma-Aldrich], 1 mM PMSF, 0.2% [wt/vol] BSA, and 1 mM DTT). Homogenization was performed on ice using a glass homogenizer (Thermo Fisher Scientific). The homogenate was centrifuged at 2,000 *g* for 10 min at 4°C, and the supernatant was centrifuged at 150,000 *g* for 45 min at 4°C to pellet microsomal membranes. For the preparation of vacuolar-enriched vesicles, the microsomal pellet was resuspended in a 15% (wt/wt) sucrose solution (containing 10 mM Tris-MES, pH 7.6, 1 mM EGTA, 2 mM DTT, 25 mM KCl, 1.1 M glycerol, 0.2% (wt/vol) BSA, 1 mM PMSF, and 1× protease inhibitor cocktail). This was then layered onto an equal volume of a 35% (wt/wt) sucrose solution (in the same buffer) and centrifuged at 150,000 *g* for 2 h at 4°C. Vesicles were collected at the gradient interface, diluted in buffer (5 mM Tris-MES, pH 7.6, 0.3 M sorbitol, 1 mM DTT, 1 mM EGTA, 0.1 M KCl, 5 mM $MgCl_2$, 1 mM PMSF, and 1× protease inhibitor cocktail), and centrifuged at 150,000 *g* for 45 min at 4°C. The final vesicle pellet was resuspend in resuspension buffer (5 mM Tris-MES, pH 7.6, 0.3 M sorbitol, 1 mM DTT, 1 mM PMSF, and 1× protease inhibitor cocktail).

Ca^{2+}/H^+ exchange activity measurements

Ca^{2+}/H^+ exchange activity was determined by measuring the Ca^{2+}-dependent dissipation of the V-ATPase–dependent pH gradient using acridine orange (Delhaize et al., 2007; Koren'kov et al., 2007). Vacuolar-enriched endomembrane vesicles (50 µg of protein) were added to a reaction buffer in a stirred cuvette containing 175 mM mannitol, 40 mM Tris-MES, pH 8.0, 50 mM KCl, 1 mM sodium azide, 100 µM sodium orthovanadate, and 5 µM acridine orange (Sigma-Aldrich) at 25°C. Fluorescence was measured upon excitation at 495 nm and emission at 540 nm using a fluorescence spectrometer (FP750; Jasco). Reactions were initiated upon addition of 2 mM ATP and 2 mM $MgSO_4$, which resulted in quench of acridine orange fluorescence upon energization of the V-ATPase. After a steady state had been achieved, 50 µM $CaCl_2$ was added in the presence of 200 nM bafilomycin-A1 (Sigma-Aldrich) to inhibit V-ATPase activity. Ca^{2+} uptake was measured as fluorescence recovery over time.

In situ hybridization

In situ hybridization on *Xenopus* embryos was performed as previously described (Harland, 1991). In brief, embryos were fixed in MOPS/EGTA/magnesium sulfate/formaldehyde buffer, dehydrated in methanol, rehydrated with PBS–0.1% Tween, treated with proteinase K, and bleached with hydrogen peroxide. Embryos were postfixed in formaldehyde and preincubated in hybridization buffer before incubation with digoxigenin-labeled RNA probes to *Twist*, *Snail2* (Linker et al., 2000), and CAX. The latter was generated from *Xenopus* IMAGE clone 6640627 (RefSeq accession no. NM_001095931.1), linearized using Pst1, and transcribed with T7 RNA polymerase. Staining was visualized using a sheep antidigoxigenin antibody coupled to alkaline phosphatase (1:3,000 dilution; Roche). Images were captured using

a stereomicroscope (MZ FLIII; Leica Biosystems) fitted with a Plan 1.0×/0.125 objective and a camera (DFC420; Leica Biosystems). Data were acquired using IM50 v5 software (Leica Biosystems).

Subcellular localization

Neural crest explants or cell lines expressing GFP-CAX with or without LAMP1-mRFP were fixed, stained with DAPI, and imaged on a confocal microscope (LSM510; ZEISS). Endogenous LAMP1 in cell lines was detected by immunocytochemistry using a primary mouse antibody raised to LAMP1 (Developmental Studies Hybridoma Bank H4A3 clone supernatant; 1:10 dilution) as described in Kilpatrick et al. (2015). In some experiments, CAX distribution was determined in live cells expressing GFP-CAX and labeled with 30–300 nM Lysotracker red or neural crest cells coexpressing mRFP-CAX and either membrane-targeted GFP or GFP–focal adhesion kinase. All images were captured using a confocal microscope (LSM-510 UV META; ZEISS) consisting of an inverted frame (AxioVert 200) and a C-Apochromat 63×/1.2 water objective. Data were acquired using LSM 510 software (ZEISS). For quantifying the distribution of mRFP-CAX relative to GFP–focal adhesion kinase, the centroid of a given GFP-positive structure was determined, and a box of 5 × 5 µm was defined around this point. Within the region of interest, the intensity of mRFP was calculated from the projected images and presented as a heat map.

In vitro migration assays

For chemotaxis assays, migration of explants to Sdf-1 was assessed using a bead assay (Theveneau et al., 2010). This was done by incubating heparin-acrylic beads (Sigma-Aldrich) overnight at 4°C in PBS supplemented with 1 µg/ml Sdf-1 and placing the beads ∼1 mm apart in a line of silicone grease (VWR) on fibronectin-coated dishes. Explants were then plated perpendicularly at a distance of 250–500 µm. To test the effects of Ca^{2+} buffering, explants were incubated for 30 min with 50 µM BAPTA-AM (Cambridge Bioscience) or EGTA-AM (AnaSpec). Time-lapse imaging was performed in Danilchick's medium using an upright microscope (Eclipse 80i; Nikon) fitted with an objective (Plan Fluor 10×/0.30 DIC L/N1) and a camera (ORCA-05G; Hamamatsu Photonics). Data were acquired using SimplePCI software. Tracking of migrating neural crest cells was performed using the ImageJ Manual Tracking plug-in. Immunocytochemistry was performed using a primary rabbit antibody to phosphopaxillin Tyr118 (1:200 dilution; EMD Millipore; Theveneau et al., 2013). Explants were costained with 2 µg/ml phallodin and 2 µg/ml DAPI.

Ca^{2+} imaging

Imaging of Ca^{2+} in SHSY5Y cells was performed using Fura-2. Cells were incubated with 2.5 µM Fura-2 AM and 0.005% vol/vol pluronic acid (Invitrogen) for 1 h in Hepes-buffered saline comprising 1.25 mM KH_2PO_4, 2 mM $CaCl_2$, 2 mM $MgSO_4$, 3 mM KCl, 156 mM NaCl, 10 mM glucose, and 10 mM Hepes, pH 7.4 (Sigma-Aldrich). Cells were imaged in Hepes-buffered saline using an inverted fluorescence microscope (IX71; Olympus) fitted with a 20×/0.75 objective (UApo/340), a monochromator light source (Polychrome IV), and a charged-coupled device camera (IMAGO; TILL Photonics). Data were acquired using TILLvisION v4. Fura-2 was excited at 340/380 nm, and emitted fluorescence was captured using a 440-nm long pass filter. Transfected cells were identified by monitoring fluorescence of the mRFP tag (excitation/emission wavelengths = 560/590 nm) before Fura-2 recording. Cells were stimulated with carbachol (Sigma-Aldrich) and GPN (Santa Cruz Biotechnology, Inc.).

Imaging of Ca^{2+} in *Xenopus* neural crest cells was performed using R-GECO1 (Zhao et al., 2011). Explants coexpressing R-GECO1 and GFP were imaged in Danilchick's medium using tissue culture dishes with cover glass bottoms (WPI FluoroDish). Fluorescence of the probes was captured upon excitation with 560-nm (for R-GECO) and 488-nm (for GFP) laser lines using a confocal microscope (Ultraview Vox; PerkinElmer) consisting of an inverted stand (TiE; Nikon) fitted with a 20×/0.75 objective (CFI Plan Apochromat VC), a spinning disk scan head (CSU-X1; Yokogawa Electric Corporation), and an electron-multiplying charged-coupled device camera (C9100-13; Hamamatsu Photonics). Data were acquired using Volocity v6.3 software. Cells were stimulated with carbachol and ionomycin (EMD Millipore). Data are presented as ratios of R-GECO1/GFP fluorescence to minimize artifacts due to cell motility.

Data analysis

All data are presented as mean and SEM from the indicated number of experiments. *, $P < 0.05$; **, $P < 0.01$; ***, $P < 0.001$.

Online supplemental material

Fig. S1 validates antisense morpholinos used in this study, shows that CAX knockdown does not affect neural crest induction, and documents prolonged association of CAX with focal adhesions. Video 1 shows that chemotaxis is disrupted upon CAX knockdown. Videos 2 and 3 show the presence of CAX-positive vesicles in protrusions and their proximity to focal adhesions, respectively. Video 4 shows that CAX knockdown reduces the lifetime of focal adhesions. Table S1 lists the yeast strains used in this study. Table S2 shows a multiple sequence alignment of animal CAXs. Online supplemental material is available at http://www.jcb.org/cgi/content/full/jcb.201510019/DC1.

Acknowledgments

We thank Olivier Cagnac, Timothy Gomez, Masa Tada, Naoto Ueno, and Kees Venema for provision of reagents, Dev Churamani and Roger Singleton Escofet for performing pilot experiments, and Bethan Kilpatrick, Ho Ney, Christopher Penny, and Lizzie Yates for comments on the manuscript.

This work was supported by the Biotechnology and Biological Sciences Research Council (grant BB/K000942/1).

The authors declare no competing financial interests.

Submitted: 6 October 2015
Accepted: 19 February 2016

References

Berridge, M.J., M.D. Bootman, and H.L. Roderick. 2003. Calcium signalling: dynamics, homeostasis and remodelling. *Nat. Rev. Mol. Cell Biol.* 4:517–529. http://dx.doi.org/10.1038/nrm1155

Brailoiu, E., D. Churamani, X. Cai, M.G. Schrlau, G.C. Brailoiu, X. Gao, R. Hooper, M.J. Boulware, N.J. Dun, J.S. Marchant, and S. Patel. 2009. Essential requirement for two-pore channel 1 in NAADP-mediated calcium signaling. *J. Cell Biol.* 186:201–209. http://dx.doi.org/10.1083/jcb.200904073

Brundage, R.A., K.E. Fogarty, R.A. Tuft, and F.S. Fay. 1991. Calcium gradients underlying polarization and chemotaxis of eosinophils. *Science.* 254:703–706. http://dx.doi.org/10.1126/science.1948048

Carmona-Fontaine, C., H.K. Matthews, S. Kuriyama, M. Moreno, G.A. Dunn, M. Parsons, C.D. Stern, and R. Mayor. 2008. Contact inhibition of locomotion in vivo controls neural crest directional migration. *Nature.* 456:957–961. http://dx.doi.org/10.1038/nature07441

Cheng, N.H., J.K. Pittman, T. Shigaki, J. Lachmansingh, S. LeClere, B. Lahner, D.E. Salt, and K.D. Hirschi. 2005. Functional association of Arabidopsis CAX1 and CAX3 is required for normal growth and ion homeostasis. *Plant Physiol.* 138:2048–2060. http://dx.doi.org/10.1104/pp.105.061218

Christensen, K.A., J.T. Myers, and J.A. Swanson. 2002. pH-dependent regulation of lysosomal calcium in macrophages. *J. Cell Sci.* 115:599–607.

Churchill, G.C., Y. Okada, J.M. Thomas, A.A. Genazzani, S. Patel, and A. Galione. 2002. NAADP mobilizes Ca^{2+} from reserve granules, lysosome-related organelles, in sea urchin eggs. *Cell.* 111:703–708. http://dx.doi.org/10.1016/S0092-8674(02)01082-6

Conn, S.J., M. Gilliham, A. Athman, A.W. Schreiber, U. Baumann, I. Moller, N.H. Cheng, M.A. Stancombe, K.D. Hirschi, A.A. Webb, et al. 2011. Cell-specific vacuolar calcium storage mediated by CAX1 regulates apoplastic calcium concentration, gas exchange, and plant productivity in *Arabidopsis*. *Plant Cell.* 23:240–257. http://dx.doi.org/10.1105/tpc.109.072769

Cunningham, K.W., and G.R. Fink. 1994. Ca^{2+} transport in *Saccharomyces cerevisiae*. *J. Exp. Biol.* 196:157–166.

Delhaize, E., B.D. Gruber, J.K. Pittman, R.G. White, H. Leung, Y. Miao, L. Jiang, P.R. Ryan, and A.E. Richardson. 2007. A role for the *AtMTP11* gene of Arabidopsis in manganese transport and tolerance. *Plant J.* 51:198–210. http://dx.doi.org/10.1111/j.1365-313X.2007.03138.x

Demaegd, D., F. Foulquier, A.S. Colinet, L. Gremillon, D. Legrand, P. Mariot, E. Peiter, E. Van Schaftingen, G. Matthijs, and P. Morsomme. 2013. Newly characterized Golgi-localized family of proteins is involved in calcium and pH homeostasis in yeast and human cells. *Proc. Natl. Acad. Sci. USA.* 110:6859–6864. http://dx.doi.org/10.1073/pnas.1219871110

Denis, V., and M.S. Cyert. 2002. Internal Ca^{2+} release in yeast is triggered by hypertonic shock and mediated by a TRP channel homologue. *J. Cell Biol.* 156:29–34. http://dx.doi.org/10.1083/jcb.200111004

Evans, J.H., and J.J. Falke. 2007. Ca^{2+} influx is an essential component of the positive-feedback loop that maintains leading-edge structure and activity in macrophages. *Proc. Natl. Acad. Sci. USA.* 104:16176–16181. http://dx.doi.org/10.1073/pnas.0707719104

Finn, R.D., J. Clements, W. Arndt, B.L. Miller, T.J. Wheeler, F. Schreiber, A. Bateman, and S.R. Eddy. 2015. HMMER web server: 2015 update. *Nucleic Acids Res.* 43:W30–W38. http://dx.doi.org/10.1093/nar/gkv397

Gietz, R.D., and R.H. Schiestl. 2007. High-efficiency yeast transformation using the LiAc/SS carrier DNA/PEG method. *Nat. Protoc.* 2:31–34. http://dx.doi.org/10.1038/nprot.2007.13

Harland, R.M. 1991. In situ hybridization: an improved whole-mount method for Xenopus embryos. *Methods Cell Biol.* 36:685–695. http://dx.doi.org/10.1016/S0091-679X(08)60307-6

Hirschi, K.D., R.G. Zhen, K.W. Cunningham, P.A. Rea, and G.R. Fink. 1996. CAX1, an H+/Ca2+ antiporter from Arabidopsis. *Proc. Natl. Acad. Sci. USA.* 93:8782–8786. http://dx.doi.org/10.1073/pnas.93.16.8782

Hooper, R., D. Churamani, E. Brailoiu, C.W. Taylor, and S. Patel. 2011. Membrane topology of NAADP-sensitive two-pore channels and their regulation by N-linked glycosylation. *J. Biol. Chem.* 286:9141–9149. http://dx.doi.org/10.1074/jbc.M110.189985

Jadot, M., C. Colmant, S. Wattiaux-De Coninck, and R. Wattiaux. 1984. Intralysosomal hydrolysis of glycyl-L-phenylalanine 2-naphthylamide. *Biochem. J.* 219:965–970. http://dx.doi.org/10.1042/bj2190965

Kilpatrick, B.S., E.R. Eden, L.N. Hockey, C.E. Futter, and S. Patel. 2015. Methods for monitoring lysosomal morphology. *Methods Cell Biol.* 126:1–19. http://dx.doi.org/10.1016/bs.mcb.2014.10.018

Koren'kov, V., S. Park, N.H. Cheng, C. Sreevidya, J. Lachmansingh, J. Morris, K. Hirschi, and G.J. Wagner. 2007. Enhanced Cd^{2+}-selective root-tonoplast-transport in tobaccos expressing Arabidopsis cation exchangers. *Planta.* 225:403–411. http://dx.doi.org/10.1007/s00425-006-0352-7

Linker, C., M. Bronner-Fraser, and R. Mayor. 2000. Relationship between gene expression domains of Xsnail, Xslug, and Xtwist and cell movement in the prospective neural crest of *Xenopus*. *Dev. Biol.* 224:215–225. http://dx.doi.org/10.1006/dbio.2000.9723

Lloyd-Evans, E., A.J. Morgan, X. He, D.A. Smith, E. Elliot-Smith, D.J. Sillence, G.C. Churchill, E.H. Schuchman, A. Galione, and F.M. Platt. 2008. Niemann-Pick disease type C1 is a sphingosine storage disease that causes deregulation of lysosomal calcium. *Nat. Med.* 14:1247–1255. http://dx.doi.org/10.1038/nm.1876

López, J.J., C. Camello-Almaraz, J.A. Pariente, G.M. Salido, and J.A. Rosado. 2005. Ca^{2+} accumulation into acidic organelles mediated by Ca^{2+}- and vacuolar H^+-ATPases in human platelets. *Biochem. J.* 390:243–252. http://dx.doi.org/10.1042/BJ20050168

López-Sanjurjo, C.I., S.C. Tovey, D.L. Prole, and C.W. Taylor. 2013. Lysosomes shape Ins(1,4,5)P3-evoked Ca^{2+} signals by selectively sequestering Ca^{2+} released from the endoplasmic reticulum. *J. Cell Sci.* 126:289–300. http://dx.doi.org/10.1242/jcs.116103

Manohar, M., H. Mei, A.J. Franklin, E.M. Sweet, T. Shigaki, B.B. Riley, C.W. Macdiarmid, and K. Hirschi. 2010. Zebrafish (*Danio rerio*) endomembrane antiporter similar to a yeast cation/H^+ transporter is required for neural crest development. *Biochemistry.* 49:6557–6566. http://dx.doi.org/10.1021/bi100362k

Mayor, R., and E. Theveneau. 2013. The neural crest. *Development.* 140:2247–2251. http://dx.doi.org/10.1242/dev.091751

Nathan, D.F., M.H. Vos, and S. Lindquist. 1999. Identification of *SSF1*, *CNS1*, and *HCH1* as multicopy suppressors of a *Saccharomyces cerevisiae* Hsp90 loss-of-function mutation. *Proc. Natl. Acad. Sci. USA.* 96:1409–1414. http://dx.doi.org/10.1073/pnas.96.4.1409

Patel, S. 2015. Function and dysfunction of two-pore channels. *Sci. Signal.* 8:re7. http://dx.doi.org/10.1126/scisignal.aab3314

Patel, S., and R. Docampo. 2010. Acidic calcium stores open for business: expanding the potential for intracellular Ca^{2+} signaling. *Trends Cell Biol.* 20:277–286. http://dx.doi.org/10.1016/j.tcb.2010.02.003

Patel, S., and S. Muallem. 2011. Acidic Ca^{2+} stores come to the fore. *Cell Calcium.* 50:109–112. http://dx.doi.org/10.1016/j.ceca.2011.03.009

Pittman, J.K. 2011. Vacuolar Ca^{2+} uptake. *Cell Calcium.* 50:139–146. http://dx.doi.org/10.1016/j.ceca.2011.01.004

Pittman, J.K., and K.D. Hirschi. 2001. Regulation of CAX1, an Arabidopsis Ca^{2+}/H^+ antiporter. Identification of an N-terminal autoinhibitory domain. *Plant Physiol.* 127:1020–1029. http://dx.doi.org/10.1104/pp.010409

Ridley, A.J., M.A. Schwartz, K. Burridge, R.A. Firtel, M.H. Ginsberg, G. Borisy, J.T. Parsons, and A.R. Horwitz. 2003. Cell migration: integrating signals from front to back. *Science.* 302:1704–1709. http://dx.doi.org/10.1126/science.1092053

Robles, E., and T.M. Gomez. 2006. Focal adhesion kinase signaling at sites of integrin-mediated adhesion controls axon pathfinding. *Nat. Neurosci.* 9:1274–1283. http://dx.doi.org/10.1038/nn1762

Scarpa, E., A. Szabó, A. Bibonne, E. Theveneau, M. Parsons, and R. Mayor. 2015. Cadherin switch during EMT in neural crest cells leads to contact inhibition of locomotion via repolarization of forces. *Dev. Cell.* 34:421–434. http://dx.doi.org/10.1016/j.devcel.2015.06.012

Spano, D., C. Heck, P. De Antonellis, G. Christofori, and M. Zollo. 2012. Molecular networks that regulate cancer metastasis. *Semin. Cancer Biol.* 22:234–249. http://dx.doi.org/10.1016/j.semcancer.2012.03.006

Stern, M.D. 1992. Buffering of calcium in the vicinity of a channel pore. *Cell Calcium.* 13:183–192. http://dx.doi.org/10.1016/0143-4160(92)90046-U

Theveneau, E., L. Marchant, S. Kuriyama, M. Gull, B. Moepps, M. Parsons, and R. Mayor. 2010. Collective chemotaxis requires contact-dependent cell polarity. *Dev. Cell.* 19:39–53. http://dx.doi.org/10.1016/j.devcel.2010.06.012

Theveneau, E., B. Steventon, E. Scarpa, S. Garcia, X. Trepat, A. Streit, and R. Mayor. 2013. Chase-and-run between adjacent cell populations promotes directional collective migration. *Nat. Cell Biol.* 15:763–772. http://dx.doi.org/10.1038/ncb2772

Tsai, F.C., and T. Meyer. 2012. Ca^{2+} pulses control local cycles of lamellipodia retraction and adhesion along the front of migrating cells. *Curr. Biol.* 22:837–842. http://dx.doi.org/10.1016/j.cub.2012.03.037

Tsai, F.C., A. Seki, H.W. Yang, A. Hayer, S. Carrasco, S. Malmersjö, and T. Meyer. 2014. A polarized Ca^{2+}, diacylglycerol and STIM1 signalling system regulates directed cell migration. *Nat. Cell Biol.* 16:133–144. http://dx.doi.org/10.1038/ncb2906

Waight, A.B., B.P. Pedersen, A. Schlessinger, M. Bonomi, B.H. Chau, Z. Roe-Zurz, A.J. Risenmay, A. Sali, and R.M. Stroud. 2013. Structural basis for alternating access of a eukaryotic calcium/proton exchanger. *Nature.* 499:107–110. http://dx.doi.org/10.1038/nature12233

Wei, C., X. Wang, M. Chen, K. Ouyang, L.S. Song, and H. Cheng. 2009. Calcium flickers steer cell migration. *Nature.* 457:901–905. http://dx.doi.org/10.1038/nature07577

Yang, J., R. Yan, A. Roy, D. Xu, J. Poisson, and Y. Zhang. 2015. The I-TASSER Suite: protein structure and function prediction. *Nat. Methods.* 12:7–8. http://dx.doi.org/10.1038/nmeth.3213

Yang, S., J.J. Zhang, and X.Y. Huang. 2009. Orai1 and STIM1 are critical for breast tumor cell migration and metastasis. *Cancer Cell.* 15:124–134. http://dx.doi.org/10.1016/j.ccr.2008.12.019

Zhao, Y., S. Araki, J. Wu, T. Teramoto, Y.F. Chang, M. Nakano, A.S. Abdelfattah, M. Fujiwara, T. Ishihara, T. Nagai, and R.E. Campbell. 2011. An expanded palette of genetically encoded Ca^{2+} indicators. *Science.* 333:1888–1891. http://dx.doi.org/10.1126/science.1208592